Annals of Nuclear Medicine (2019) 33:459–470
https://doi.org/10.1007/s12149-019-01353-w

ORIGINAL ARTICLE

A systematic performance evaluation of head motion correction techniques for 3 commercial PET scanners using a reproducible experimental acquisition protocol

Takato Inomata[1] · Shoichi Watanuki[2] · Hayato Odagiri[3] · Takeyuki Nambu[4] · Nicolas A. Karakatsanis[5] · Hiroshi Ito[4,6] · Hiroshi Watabe[7] · Manabu Tashiro[2] · Miho Shidahara[2,8]

Received: 26 January 2019 / Accepted: 22 March 2019 / Published online: 29 March 2019

Abstract

Purposes Subject's motion during brain PET scan degrades spatial resolution and quantification of PET images. To suppress these effects, rigid-body motion correction systems have been installed in commercial PET scanners. In this study, we systematically compare the accuracy of motion correction among 3 commercial PET scanners using a reproducible experimental acquisition protocol.

Methods A cylindrical phantom with two ^{22}Na point sources was placed on a customized base to enable two types of motion, 5° yaw and 15° pitch rotations. Repetitive PET scans (5 min × 5 times) were performed at rest and under 2 motion conditions using 3 clinical PET scanners: the Eminence STARGATE G/L PET/CT (STARGATE) (Shimadzu Corp.), the SET-3000 B/X PET (SET-3000) (Shimadzu Corp.), and the Biograph mMR PET/MR (mMR) (Siemens Healthcare) systems. For STAR GATE and SET-3000, the Polaris Vicra (Northern Digital Inc.) optical tracking system was used for frame-by-frame motion correction. For Biograph mMR, sequential MR images were simultaneously acquired with PET and used for LOR-based motion correction. All PET images were reconstructed by FBP algorithm with 1 × 1 mm pixel size. To evaluate the accuracy of motion correction, FWHMs and spherical ROI values were analyzed.

Results The percent differences (%diff) in averaged FWHMs of point sources at 4 cm off-center between motion-corrected and static images were 0.77 ± 0.16 (STARGATE), 2.4 ± 0.34 (SET-3000), and 11 ± 1.0% (mMR) for a 5° yaw and 2.3 ± 0.37 (STARGATE) and 1.1 ± 0.60 (SET-3000) for a 15° pitch respectively. The averaged %diff between ROI values of motion-corrected images and static images were less than 2.0% for all conditions.

Conclusions In this study, we proposed a reproducible experimental framework to allow the systematic validation and comparison of multiple motion tracking and correction methodologies among different PET/CT and PET/MR commercial systems. Our proposed validation platform may be useful for future studies evaluating state-of-the-art motion correction strategies in clinical PET imaging.

Keywords Brain PET · Motion-correction · PET/MR · Optical tracking · Reproducibility

Introduction

Normally, clinical brain PET scan protocols require the subjects to lie still on the bed with head fixation until the end of the scan. However, involuntary rigid motions may briefly, or continuously, occur during the scan thereby resulting in changes of position/posture on the bed due to disease symptoms, comfort loss and execution of neurological tasks among other reasons. These types of motion during the brain PET scan can degrade spatial resolution and quantification of PET images [1]. Previously, rigid-body motion correction techniques for brain PET have been investigated to measure the subject's motion during acquisition and correct for its effects during data processing [1–22].

To measure the subject's motion, data-driven methods have previously been introduced using list-mode PET data [23, 24], dynamic PET images [11, 17, 19], sequential MR images acquired simultaneously with PET [2, 4, 18], marker tracking methods with optical devices [1, 20–22] or

✉ Miho Shidahara
miho.shidahara@qse.tohoku.ac.jp

Extended author information available on the last page of the article

radioactive- or MR-active markers [9, 16], and marker-less tracking methods where the object's surface features can be extracted with CCD cameras [10, 15, 25] or with Microsoft Kinect [7]. Recently, the estimation of the object's motion during iterative-reconstruction has also been proposed [6].

The measured motion can subsequently be corrected for each line-of-response (LOR) of the list-mode data or for each sinograms/reconstructed image of a collection of scan time frames. LOR-based motion correction (also known as event-by-event motion correction) with fine sampling of subject motion can achieve high accuracy and time-resolution [13]. Each coincidence event detected in a certain LOR can be reassigned to the correct LOR together with the proper random and normalization correction factors from the detected LOR position and then rebinned into a motion corrected sinogram. Then, conventional attenuation and scatter correction factors corresponding to the corrected LOR positions can be applied. Alternatively, event-by-event motion compensation can be implemented within a list-mode reconstruction framework as it was previously proposed (MOLAR) [12]. Even though event-by-event is considered the gold-standard methodology for accurate motion correction, it requires large computational time proportional to the number of detected coincidence events. Multi-frame sinogram-based and image-based motion correction techniques (also known as frame-by-frame motion correction) can be a more practical approach, in terms of computational time, than event-by-event, but requires either a frame-classification according to the subject's motion profile or a fixed time frame/interval [26, 27]. For accurate attenuation and scatter correction, the attenuation map at the original position should be transformed into the moved position of each frame by applying averaged motion parameters within each frame. Subsequently, the image reconstructions with the transformed attenuation and scatter correction factors are performed for each frame-sinogram. Finally, the reconstructed PET images are transformed back and summed into the reference image position to produce the motioncorrected PET image [1]. In case of multi-frame dynamic PET images, at first each frame image is reconstructed without attenuation and scatter correction and then registered into the reference image to estimate the corresponding motion parameters [11]. Then, the attenuation correction and scatter correction factors can be transformed to each frame position using the previously estimated motion parameters [11]. However, the accuracy of the estimated motion parameters at each frame depends on the signal-to-noise ratio of the corresponding reconstructed dynamic image, which can be considerably low for frames with very short time intervals.

A variety of approaches and their combinations have been previously proposed for measuring the subject's motion during a PET acquisition and utilizing this information to process the acquired data afterwards and correct for the measured motion. Although the accuracy of some of these combinations were previously reported [15, 18, 20, 28, 29], however, the objective and systematic comparison of the accuracy between these methodologies may not be feasible, as the evaluations were based on unique PET datasets with unique object's motion. To compare the basic performance metrics of various motion correction approaches among different PET scanners, the evaluated PET datasets should be acquired with similar conditions and the object's motions should be as consistent as possible to ensure "reproducibility" of the findings and extraction of useful conclusions for future studies.

Recently, motion correction systems have been installed in commercial PET scanners. However, the systematic comparison of the accuracy of motion correction among PET scanners through a common validation protocol has not been reported yet. In this study, we propose a highly reproducible validation protocol to systematically evaluate the accuracy of motion correction capabilities among 3 PET commercial scanners and present our validation results to be further utilized by future brain PET studies.

Material and methods

PET scanners

Three commercial PET scanners equipped with motion correction systems, Eminence STARGATE G/L, SET-3000 B/X (Shimadzu Corp., Kyoto, Japan) and Biograph mMR (Siemens Healthcare, Erlangen, Germany) were used in this study. STARGATE is PET/CT scanner and consists of 4 rings of 88 detector blocks, each of which is divided into 9×10 gadolinium oxyorthosilicate (GSO) crystals ($2.45 \times 5.1 \times 30$ mm). The axial field of view (FOV) is 20.8 cm, and the transverse FOV is 60 cm. SET-3000 is a standalone PET scanner and consists of 5 rings of 88 detector blocks, each of which is divided into 6×8 bismuth germanium oxide (BGO) crystals ($3.5 \times 6.25 \times 30$ mm). The axial FOV is 26 cm, and the transverse FOV is 60 cm. Both STARGATE and SET3000 are equipped with an optical tracking system by Polaris Vicra (Northern Digital Inc., Ontario, Canada) for motion tracking with 20 Hz sampling-pitch. Moreover, in both systems a multi-frame sinogram-based motion correction with manual frame-classification was implemented [30]. Biograph mMR is a PET/MRI scanner and consists of 8 rings of 56 detector blocks, each of which is divided into 8×8 lutetium oxyorthosilicate (LSO) crystals ($4 \times 4 \times 20$ mm). The axial FOV is 25.8 cm, and the transverse FOV is 59.4 cm. An MR-driven PET motion correction system was installed that synchronizes the PET data with simultaneously acquired MR data every TR = 1 s (1 Hz sampling-pitch) [18]. The acquired MR data are immediately

reconstructed and registered to the first MR volume, which is considered as the reference frame, to estimate the motion data. Subsequently, an LOR-based motion correction algorithm was implemented.

Experimental protocols

To evaluate the accuracy of motion correction, PET scans of a cylindrical object were performed for each scanner while a specific type of rigid motion was applied to the object. Figure 1a shows an overview of the experimental phantom set-up. The cylindrical acrylic phantom (inner ϕ 21 cm$\times L$ 21 cm, 0.5 cm thickness) was filled with water. An acrylic disk insert was placed in transaxial orientation at the phantom's axial center. Two ^{22}Na point sources (ϕ 0.25 mm) were sealed within 1 cm^3 acrylic cubes (Type: MMS09, Eckert&Ziegler co. Ltd) (0.456 and 0.102 MBq) and attached to the acrylic disk insert (ϕ 20 cm$\times T$ 0.5 cm) at 4 and 8 cm off-center, respectively (Fig. 1b). To move the phantom, we also made an in-house acrylic base as illustrated in Fig. 1c. This base enabled the phantom's rotation around its body axis (yaw) or its horizontal axis (pitch). For yaw rotation, the phantom was placed on top of the base and rotated in 5° increments using a marked wooden stick (ϕ 2 cm$\times L$ 115 cm) attached to the side of the cylinder (Fig. 1b). For the 15° pitch rotations, a rectangular spacer was inserted as shown Fig. 1c. In the case of STARGATE and SET-3000 systems, the target markers for motion tracking were also attached to the bottom of the phantom.

Data acquisition

We performed phantom experiments with rest and 2 types of motion (5°-yaw and 15°-pitch) for each PET scanner according to the scheme illustrated in Fig. 2a, except for the 15°-pitch for the mMR scanner.

For STARGATE and SET-3000, after 5-min transmission scans with ^{137}Cs (683 and 623 MBq, respectively) [31], 5 repetitive emission scans of 5 min each were performed at the rest condition using the energy window of 400–624 keV (STARGATE and SET-3000) and a coincidences time window of 6 ns (STARGATE) and 10 ns (SET-3000). The phantom was manually replaced at initial position before every scan started. Furthermore, to investigate the reproducibility between different days of experiments, an additional set of 5 repetitive emission scans at the rest conditions was performed at a different day. Furthermore, two sets of 5 repetitive emission scans of 5 min each were performed with each set corresponding to one of 2 types of motion conditions. For the first motion condition, a 5° yaw rotation, the phantom was manually rotated 5° using a wooden stick at 2.5 min after starting the scan and kept its position until the end of the scan. For the second motion condition, a 15° pitch rotation, the phantom was manually rotated 15° by inserting a spacer of appropriate size (Fig. 1c) at 2.5 min after starting the scan and kept its position until the end of the scan. For both motion-conditions, before the next scan started, the phantom was manually replaced at its initial position. All phantom motions were measured during each emission scan.

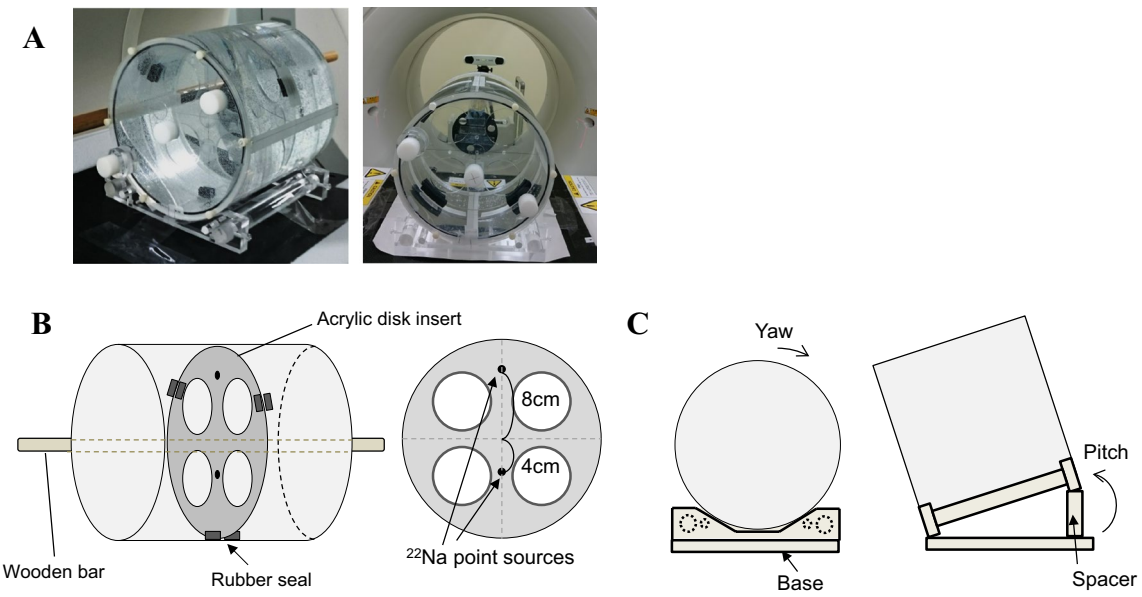

Fig. 1 Overview of the experimental phantom, **a** photograph, **b** geometry inside the phantom: acrylic disk insert attached with two ^{22}Na point sources and positioned at the phantom's central transaxial plane, **c** phantom motion mechanisms of yaw and pitch rotations

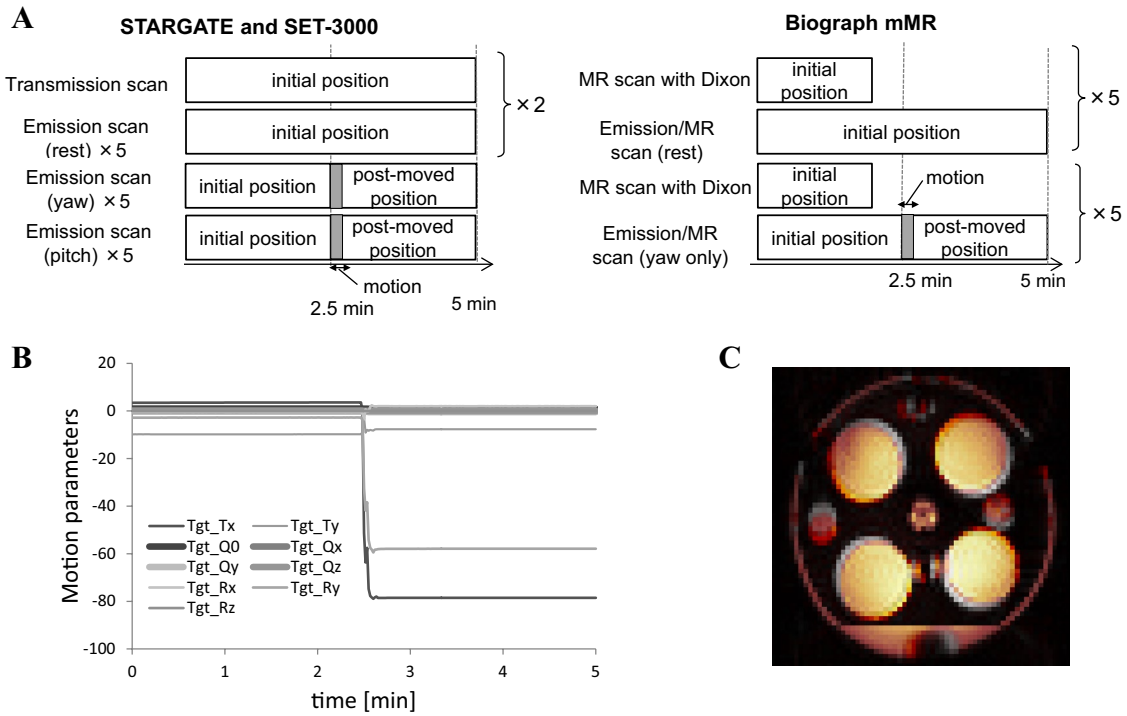

Fig. 2 Experimental protocols, **a** time-courses of PET experiments for STARGATE, SET-3000 and Biograph mMR, **b** example of motion-parameters measured by Polaris, and **c** example of two MR Dixon images of the phantom anatomy before (gray) and after (hot) motion acquired by Biograph mMR

Figure 2b shows an example of a set of measured motion-parameters by the STARGATE system.

For Biograph mMR, a series of Dixon MR scans (TR: 3.6 ms, TEopp: 1.23 ms, TEin: 2.46 ms) were performed at the phantom's initial position for attenuation correction before the beginning of every emission scan [32]. repetitive emission scans using the energy window of 430–610 keV and a coincidences time window of 5.86 ns were performed with the Biograph mMR system at rest and for a 5° yaw rotation, similarly to the scans performed with the STARGATE and SET-3000 systems. The phantom motion was monitored by simultaneously acquired MR images at 1 s intervals (TR: 1 s, TE: 0.3 s, Voxel size: 3.8 × 3.8 × 3.0 mm). Figure 2c shows the example of two phantom MR images before (gray-scale) and after (hot-scale) phantom motion.

Image reconstruction and motion correction

We employed for all 3 PET scanners the filtered back projection (FBP) reconstruction algorithm without post-filter (1 × 1 mm pixel size), including both attenuation and scatter corrections (AC and SC). The ACs were performed with μ-maps generated from transmission scans, in the case of STARGATE and SET-3000 systems, or Dixon-based MR scans, in the case of the Biograph mMR system [31, 32]. SCs were performed with convolution-subtraction, for the STARGATE and SET-3000 systems [31], or single-scatter-simulation for the Biograph mMR system [32].

For the STARGATE and SET-3000 systems, a frame-by-frame motion correction approach was followed. The list-mode PET data of each scan were manually divided into 4 frames, namely the reference, uncorrected, rejection and corrected frames, based on measured motion parameters as shown in Fig. 2b. The Reference frame corresponded to the first 20 s after the scan start, while the Uncorrected frame was defined from 20 s to 2.5 min after the scan start, followed by the rejection frame from 2.5 min to the time the motion was completed. Finally, the Corrected frame, which was the target for motion correction in this study, corresponded to the scan period beginning from the time the motion was completed to the end of the scan. The acquired list-mode PET data of the reference, uncorrected and corrected frames were rebinned into a corresponding set of sinogram frames. Both the Reference and the Uncorrected sinograms were reconstructed with AC and SC derived by the μ-map at the reference position. However, the Corrected sinograms was reconstructed with AC and SC derived by the μ-maps transformed according to the measured phantom motion. Finally, the motion-corrected PET images were transformed to the reference and then all reference, uncorrected and corrected images were summed into a static motion corrected image.

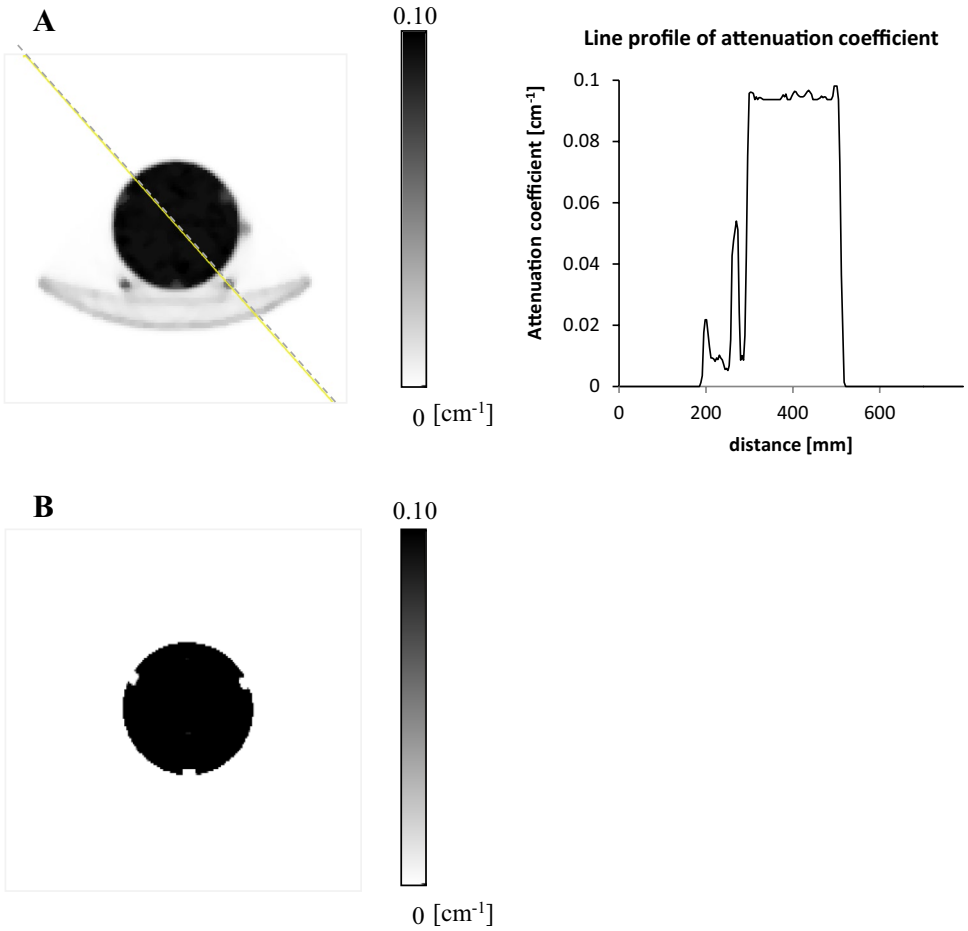

Fig. 3 Central transaxial slices and line profiles of the μ-maps of the experimental phantom for **a** STARGATE, and **b** Biograph mMR systems

For Biograph mMR, LOR-based motion correction was performed [18]. The motion was accounted for in the LOR space by moving the coordinates of all crystal based on the transformation matrix of 300 frames (TR of 1 s and a total PET scan of 5 min), while setting the reference location as the one corresponding to the first 1 s after the scan start. The transformed events were rebinned into prompt and delayed sinograms of 300 frames. Finally, the random, attenuation and scattercorrected sinograms were summed into a single frame and then reconstructed as a static motion corrected image.

Data analysis

To evaluate the effect of motion correction on the spatial resolution, we assessed in static (rest) and motion corrected PET images ($n = 10$ for the static acquisitions with STARGARE and SET-3000, $n = 5$ for the remaining acquisitions) the averaged FWHMs (mm) of the activity distributions of two ^{22}Na point sources, at 4 and 8 cm off-center respectively, by fitting line profiles in the horizontal (X), vertical (Y) and axial (Z) direction with an 1-dimensional Gaussian function. Furthermore, we calculated the percent differences of the averaged FWHMs in motion corrected images against those in the rest images as follows:

$$\%\text{difference} = \frac{\text{FWHM}_{\text{MC}} - \text{FWHM}_{\text{rest}}}{\text{FWHM}_{\text{rest}}} \times 100, \quad (1)$$

where FWHM_{MC} and $\text{FWHM}_{\text{rest}}$ are FWHMs of motion corrected PET image and PET image at rest, respectively.

To evaluate the quantification before and after motion correction, in terms of counts-preservation, ROI analysis was also performed by drawing spherical ROIs with 3 cm diameter on the PET images of each of the two ^{22}Na point sources. Total ROI counts (cps) of motion corrected images were compared with that of the rest images. Percent differences of ROI counts in motion corrected images against those in the rest images were also calculated according to Eq. (1).

To evaluate the reproducibility of phantom-positioning, %COV (= 100 × 1 S.D/Mean) of the FWHMs were also calculated for rest and motion corrected images ($n = 10$ for the static acquisitions with STARGARE and SET-3000, $n = 5$ for the remaining acquisitions).

Results

μ maps for attenuation correction

Figure 3a shows the μ-map of the experimental phantom as obtained from STARGATE with a transmission scan. Not only the phantom itself but also other medium (bed, base and wooden bar) were visually observed in μ-map, however, the line profiles of μ-map indicates that the μ values of both the base and bed were lower than that of phantom itself. Figure 3b shows μ-map of experimental phantom in Biograph mMR. Even though the slice of μ-map in Fig. 3b corresponds to the acrylic disk insert of Fig. 1b, we confirmed that μ values of water were assigned inside segmented phantom except for rubber seals.

Phantom-motion during PET scan

In this study, phantom-motion was implemented by manual handling. For 5°-yaw, the required time for phantom-motion in STARGATE, SET-3000 and Biograph mMR were 6.8 ± 0.75, 6.2 ± 1.2 s, and 8.0 ± 1.1 s, respectively. For 15°-pitch, the required time for phantom-motion in STAR GATE and SET-3000 were 11 ± 1.5 and 11 ± 1.5 s, respectively. For each 5°-yaw and 15°-pitch, no significant differences in time was observed among the 3 PET scanners (t test, $p < 0.05$).

Figure 4 shows PET images before and after motion correction of PET acquisitions with STARGATE, SET-3000 and mMR scanners. For both the 5° yaw and 15° pitch rotations, each ^{22}Na point source was observed at 2 positions in the uncorrected PET images, while it is visually evident that motion correction mitigated the effects on spatial resolution in the corrected PET images for all 3 PET scanners.

Accuracy of motion correction

As shown in Table 1, the average $FWHM_{rest}$ of the ^{22}Na point sources in x-direction at 4 and 8 cm off-center was 5.3 ± 0.011 and 5.4 ± 0.010 (STARGATE), 5.6 ± 0.021 and 5.8 ± 0.016 (SET-3000), and 4.0 ± 0.011 and 4.2 ± 0.020 mm (mMR), respectively. For all types of motion, the $FWHM_{MC}$ did not perfectly match the $FWHM_{rest}$. As shown in Fig. 5a, c, e in the case of the 5° yaw rotation, the average % differences between $FWHM_{MC}$ and $FWHM_{rest}$ were larger in Biograph mMR than

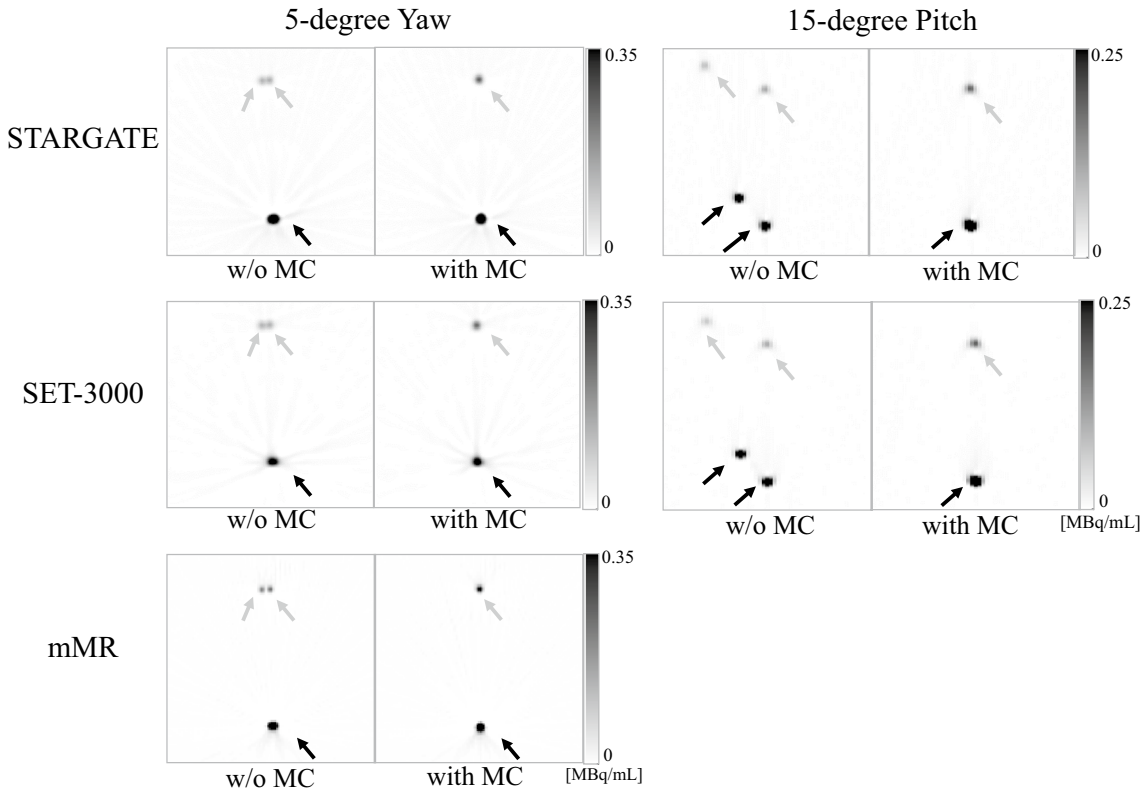

Fig. 4 Two left columns: Transaxial views of the central slice of PET images before and after motion correction of 5° yaw rotations with STARGATE, SET-3000 and Biograph mMR systems. Two right columns: Sagittal views of PET images before and after motion correction of 15° pitch rotations with STARGATE and SET-3000 systems. The black and gray arrows indicate ^{22}Na point sources at 4 and 8 cm off-center, respectively

Table 1 Summary of average FWHM (mm) performance for rest and motion corrected ^{22}Na point source images as obtained from PET scans with STARGATE, SET-3000 and Biograph mMR scanners ($n=10$ for the rest experiments of STARGATE and SET-3000, $n=5$ for the other experiments)

Position of point source	Index	Conditions	STARGATE			SET-3000			Biograph mMR		
			Average	SD	%COV	Average	SD	%COV	Average	SD	%COV
4 cm	FWHM (*x*)	Rest	5.32	0.011	0.20	5.64	0.021	0.38	4.02	0.011	0.28
		MC-yaw	5.36	0.009	0.16	5.78	0.019	0.33	4.47	0.042	0.93
		MC-Pitch	5.44	0.020	0.36	5.70	0.034	0.59	–	–	–
	FWHM (*y*)	Rest	5.41	0.013	0.24	5.54	0.014	0.26	4.49	0.012	0.28
		MC-yaw	5.47	0.011	0.20	5.61	0.005	0.09	4.89	0.014	0.29
		MC-Pitch	5.64	0.019	0.34	5.88	0.089	1.51	–	–	–
	FWHM (*z*)	Rest	6.20	0.046	0.75	6.67	0.039	0.58	5.34	0.084	1.58
		MC-yaw	6.36	0.035	0.55	6.78	0.011	0.17	5.67	0.044	0.78
		MC-Pitch	6.34	0.123	1.93	6.96	0.141	2.03	–	–	–
8 cm	FWHM (*x*)	Rest	5.44	0.010	0.19	5.75	0.016	0.27	4.22	0.019	0.44
		MC-yaw	5.54	0.028	0.51	5.92	0.019	0.32	4.59	0.020	0.43
		MC-Pitch	6.51	0.041	0.62	5.85	0.033	0.57	–	–	–
	FWHM (*y*)	Rest	5.81	0.025	0.44	5.77	0.028	0.48	4.82	0.021	0.43
		MC-yaw	5.88	0.024	0.41	5.85	0.020	0.34	5.07	0.022	0.43
		MC-Pitch	6.17	0.064	1.04	6.35	0.103	1.62	–	–	–
	FWHM (*z*)	Rest	6.47	0.027	0.41	7.39	0.032	0.43	5.43	0.036	0.67
		MC-yaw	6.51	0.041	0.62	7.43	0.035	0.47	5.60	0.060	1.07
		MC-Pitch	6.81	0.138	2.03	8.00	0.107	1.34	–	–	–

in STARGATE and SET-3000 systems. In the case of the 15° pitch rotation, the average % differences between $FWHM_{MC}$ and $FWHM_{rest}$ were larger in *y* and *z* directions (Fig. 5d, f) than in *x* direction (Fig. 5b). Meanwhile, the % FWHM differences were larger for the SET-3000 system in *y* and *z* directions and similar to the STARGATE system in the *x* direction.

Moreover, as shown in Fig. 6, the average % difference in ROI values between motion-corrected and rest images were less than 2.0% for all types of motion.

Reproducibility of present experiments

As shown in Table 1, at rest, the %COVs of $FWHM_{rest}$ were less than 1.6% (maximum value was measured for mMR in the *z*-direction, at 4 cm off-center). After motion correction, the %COVs of $FWHM_{MC}$ were, regardless of the motion type, less than 2.0% (maximum values were measured for STARGATE in the *z*-direction, at 8 cm off-center, with 15° pitch rotation and for SET3000 in the *z*-direction, at 4 cm off-center, with 15° pitch rotation).

Discussions

The correction of subject's motion during PET scans can contribute to improvement in quantification as previously suggested by a range of proposed methodologies [1–22]. However, the performance evaluation of each motion correction technique has been conducted with different objects and types of motion thus challenging the drawing of useful conclusions concerning comparisons between the different approaches. In this study, we presented a series of phantom experiments as a common validation platform to systematically and objectively evaluate the accuracy of motion correction strategies in 3 commercial PET scanners. The phantom experiment protocols were carefully designed such that a high degree of reproducibility of the experimental conditions can be achieved thereby allowing their utilization by future studies.

Proposed phantom and protocols

As shown in Fig. 1, we set a cylindrical phantom with two ^{22}Na point sources on a special base designed to apply reproducible types of motion. For PET imaging, the object has to contain positron-emitting radioisotopes. However, the filling of a phantom with a radioactive solution of short half-life is expected to diminish reproducibility between experiments. Moreover, point sources of very small diameters can also affect reproducibility, because they are regarded as sensitive to slight movements. Therefore, for our proposed validation platform we used sealed point sources of ^{22}Na with a long half-life (2.602 years) and a moderately small diameter (e.g. 0.25 mmϕ).

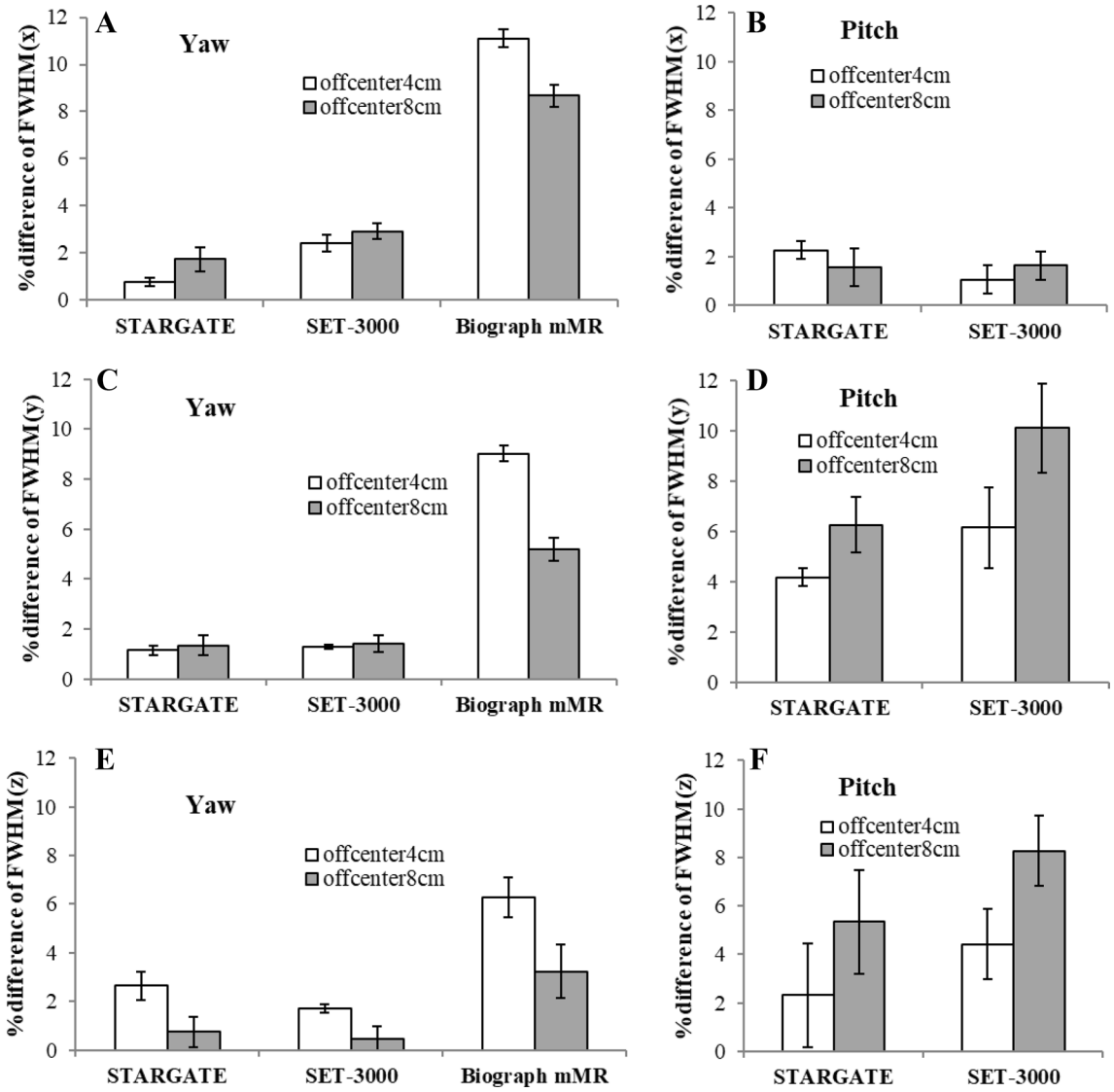

Fig. 5 Average % differences in FWHM ($n=5$) between motion corrected and rest (static) PET images for **a** 5° yaw rotations in *x*-direction, **b** 15° pitch rotations in *x*-direction, **c** 5° yaw rotations in *y*-direction, **d** 15° pitch rotations in *y*-direction, **e** 5° yaw rotations in *z*-direction, and **f** 15° pitch rotations in *z*-direction

Furthermore, we evaluated the accuracy of different motion correction strategies in both PET and PET/MRI clinical scanners using a common experimental phantom. In the case of PET/MRI experiments, the phantom motion was measured through sequential MR images acquired simultaneously to the PET images. For estimating the motion in our Biograph mMR system, we implemented a rigid registration method between the target and reference MR images using intensity differences. In the case of 5° yaw rotations, two frame MR images of a cylindrical phantom at different positions may result in no differences therefore yielding to erroneous motion measurements. To avoid this, we used an acrylic disk insert with 4 holes (Fig. 1b), thus enabling the motion detection from rotating MR images and the successful motion correction of PET data acquired with the Biograph mMR scanner (Table 1).

To evaluate the reproducibility of our phantom experiments, we repeated the PET scans 5 times for each experiment with and without phantom-motion. Before every scan, the phantom was placed at its initial position manually. At rest, in particular, we performed 5 repetitive emission scans at 2 different days resulting in a %COV range of 0.19–1.6% ($n=10$) for the $FWHM_{rest}$ (Table 1). Furthermore, for the 5° yaw and 15° pitch rotation, the %COV for $FWHM_{MC}$ ($n=5$) ranged 0.093–2.0% (Table 1), which is similar to the range achieved at rest. We also confirmed that there were no significant differences between the duration of the motion applied to the scans of all 3 PET scanners.

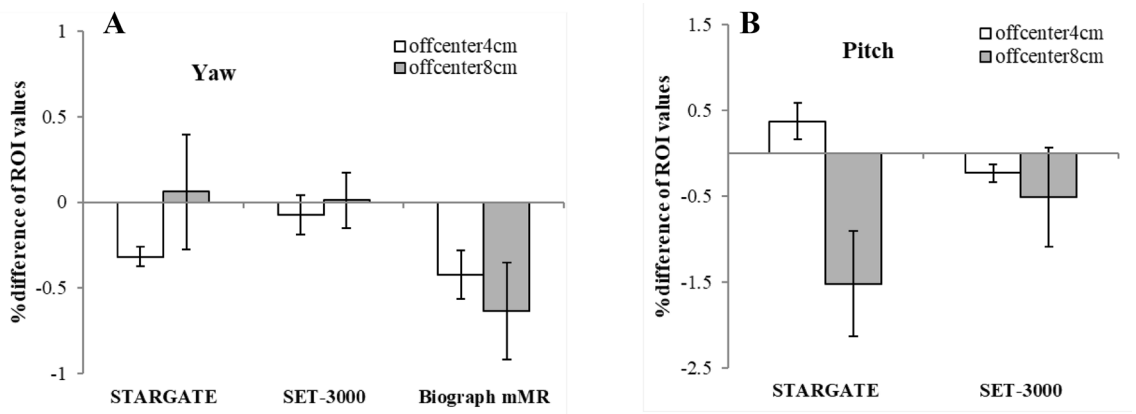

Fig. 6 Average %difference in ROI values ($n = 5$) between motion corrected and rest (static) PET images for **a** 5° yaw and **b** 15° pitch rotations

Mismatch of μ maps

In this study, we observed mismatches between the true and the applied μ maps for attenuation correction in terms of segmentation and location. For the Biograph mMR, the attenuation of photons caused from the bed, as well as from the base and wall (5 mm thickness) of the cylindrical phantom were not corrected as shown in Fig. 3b. For both STAR TGATE and SET-3000, the attenuation of photons caused from the cylindrical phantom was corrected in the motion-corrected frame. However, the attenuation of photons from the bed and the base were not accurately corrected, because the whole μ map, as opposed to the moving phantom only, in Fig. 3a was transformed to the moved-position for attenuation correction. In the present study, we used point sources and were able to confirm the counts preservation before and after motion correction, thereby suggesting that the observed μ map mismatches did not affect quantification significantly. However, if the distribution of the radioisotope was different from that of the present study, the mismatch may have had a more significant effect on PET quantification.

Comparison of the accuracy of motion correction

The intrinsic spatial resolution, as measured by the average $FWHM_{rest}$ metric, was better for the Biograph mMR than for the STARTGATE and SET-3000 systems (Table 1). We confirmed that the measured $FWHM_{rest}$ values are comparable with previous reports of performance evaluation [33, 34]. For the 3 PET scanners, all FWHMs were improved after motion correction and total counts were preserved before and after motion correction. However, for the 5° yaw rotation, the improvement of $FWHM_{MC}$ was smaller for the Biograph mMR than for the STARGATE and SET-3000 systems (Fig. 5a, c, e). This may have been caused by the relatively poor sampling motion rate of every 1 s in the Biograph mMR experiments, or the large pixel size of the simultaneously acquired co-registered MR images. As a preliminary test, we performed motion correction for the rejection frame data acquired with STAR GATE using a motion sampling interval of 1 s for 5° yaw rotations, however, significant effect of the %difference between $FWHM_{MC}$ and $FWHM_{rest}$ was not observed (data not shown), a motion sampling interval of 1 s did not ffect the %difference of $FWHM_{MC}$ in this study. The pixel size of the simultaneously acquired MR image for estimating phantom motion was 3.8×3.8 mm while the reconstructed PET image voxel size was 1×1 mm. We should note that the pixel size of the MR images may influence the accuracy of the estimated motion, which, in turn, can propagate to the $FWHM_{MC}$ results. The same effect is expected for the pixel size of the PET images. For mMR, if the pixel size of the PET images was larger or equivalent to that of the MR image, the $FWHM_{rest}$ of the point source in the PET images would have deteriorated. Thus, in this case the %diff index would have been less sensitive for evaluating any quantitative differences in the spatial resolution between static images and images corrected with different motion correction.

For the 15° pitch rotations, even though the same optical tracking system and pixel size of reconstructed images (1×1 mm in trans-axial plane) were used, the % difference between $FWHM_{MC}$ and FWHMrest was lower in STARGATE than in SET-3000 (Fig. 5d, f). Furthermore, these %differences for the 15-dgree pitch rotations were larger than those for the 5° yaw rotations especially in *y*- and *z*-directions. Different performance metrics maybe triggered due to differences in the slice thickness between the two PET scanners: 2.6 mm for STARGATE and 3.25 mm for SET-3000 systems. The aforementioned quantitative performance metrics could be comparatively evaluated only through our proposed reproducible experimental acquisition protocols.

The derived conclusions can thus be quite useful for further performance evaluation comparisons in future studies.

Limitation of the study

In this study we focused the comparison on optical and MR data-driven motion tracking techniques for PET acquisitions. Thus, we designed our experimental phantom according to the demands of these two motion-tracking techniques in particular. As a result, the proposed phantom may not be appropriate for evaluating other types of motion tracking, such as techniques using CCD images and features extraction. Nevertheless, our phantom can be adapted to support feature extraction from its surface and later be used for evaluation of such motion tracking strategies. We also used FBP as an image-reconstruction algorithm for evaluating the FWHMs metrics. However, model-based statistical iterative reconstruction methods (e.g. MOLAR) could instead be used in future. Even though our proposed phantom supports two types of motion (yaw and pitch), we could not perform experiments with pitch-motion for the Biograph mMR experiments. This is due to the long axial length of the mMR integrated PET/MR gantry, which prevented any manual application of the pitch rotation without moving the bed during the PET acquisition. On the contrary, pitch rotation could be easily applied during the PET scan in the shorter gantries of the STARGARE and SET-3000 systems without moving the bed. As the pitch motion experiment could not be accurately reproduced in the mMR scanner, we decided to evaluate pitch motion correction performance only for the STARGATE and SET-3000 systems. However, total-body bore PET scanners with 2-meter long fields-of-view have recently been developed [35, 36], where manual pitch-motion evaluation without moving the bed position could be challenging in future. One potential solution would have been to acquire two consecutive PET acquisitions, one before and one after applying the pitch-rotation motion, and then estimate and correct the motion between the two PET data frames. Of course, in that case, any emission data during the motion application would be missing. In general, our proposed phantom can be adopted to most clinical and research PET scanners. We should note that STARGATE is PET-front PET/CT system whereas conventional PET/CT scanners are usually front-CT system. In cases of CT-front PET/CT system, we can generate the same yaw and pitch rotations from the back-side in the same way of STARGAT E.

In this study, two types of motions, yaw- and pitch rotations, were selected to mimic the subject's head shaking and nodding respectively. Both types of motion are likely to occur during a human brain PET exam. We selected the yaw-rotation to simulate the shaking of brain. The 5° extent of motion was preferred based on a previous investigation of brain PET motion correction approaches by Bloomfield et al. [1]. Moreover, our decision was also determined by the restriction of the motion tracking algorithm in the mMR for less than 8° rotation angles. Similarly, we considered that a 15° pitch rotation (nodding) also reflect a possible extent of head nodding for humans when lying on a scanner table.

Furthermore, we employed cylindrical phantoms to assess the performance of different systems to correct for these motion effects. In the case of phantoms, we expect the effects of rigid motion not to vary significantly across the different phantom regions and primarily depend on the distance of the phantom regions from the center of the rotations. Therefore, we consider that the two measurement points at 4 cm and 8 cm off-center were sufficient for the purposes of this phantom evaluation study. However, in clinical PET studies, where the administered radiotracers may be distributed over a wider area forming a variety of contrast features, a larger set of carefully selected measurement sites would be needed.

In this study, we used a simple cylindrical phantom with two point sources and a reproducible motion application mechanism to systematically evaluate and compare the accuracy of different motion correction techniques across commercial PET systems. In our evaluation we applied simple types of rotations likely to occur in human brain PET studies on phantoms of known activity concentration. On the other hand, in clinical PET studies the true activity concentration is unknown. The use of this less complex set-up ensured experimental conditions that can be easily reproduced by future investigators. Furthermore, the effect of more complex types of rigid motion on phantoms are not expected to be significantly different due to the presence of large regions of uniform activity concentrations in phantoms. Instead of complexity, we focused in this study on reproducibility and the knowledge of the true activity concentration. Our approach allowed us to more systematically assess the relative performance of different motion correction systems on real data acquired by clinical PET scanners. We thus believe that our findings can be useful for future clinical studies targeting brain PET imaging and motion correction. Besides, in order to assess the accuracy of motion correction for clinical subjects with specific diseases, we would need to perform more complex types of rigid motion and evaluate additional motion patterns (speed, irregularity and amplitude). However this is outside the current scope of our study but will be considered as future work.

Conclusion

In this study, we proposed a reproducible experimental framework to allow the systematic validation and comparison of multiple motion tracking and correction methodologies among different PET/CT and PET/MR commercial

systems. Our findings suggest a strong dependence of the motion correction accuracy on the quality of the object's motion monitoring, the scanner geometry, and the types of motion occurring during a PET scan. Our quantitative performance metrics were comparable between the different acquisitions thanks to the reproducibility of our experimental acquisition protocols. Therefore, our proposed validation platform may be useful for future studies evaluating state-of-the-art motion correction strategies in clinical PET imaging.

Acknowledgement We would like to thank the research staff at Advanced Clinical Research Center, Fukushima Medical University for helpful support to our experiments. This study was supported in part by Grants-in-Aid for Scientific Research (C) (No. 15K08687) and (B) (No 17H04118) from the Ministry of Education, Culture, Sports, Science and Technology (MEXT), Japanese Government.

Funding This study was supported in part by Grants-in-Aid for Scientific Research (C) (No. 15K08687) and (B) (No 17H04118) from the Ministry of Education, Culture, Sports, Science and Technology (MEXT), Japanese Government.

Compliance with ethical standards

Conflict of interest All authors declare that they have no conflict of interest.

References

1. Bloomfield PM, Spinks TJ, Reed J, Schnorr L, Westrip AM, Livieratos L, et al. The design and implementation of a motion correction scheme for neurological PET. Phys Med Biol. 2003;48(8):959–78.
2. Reilhac A, Merida I, Irace Z, Stephenson M, Weekes A, Chen C, et al. Development of a dedicated rebinner with rigid motion correction for the mMR PET/MR scanner, and validation in a large cohort of ^{11}C-PIB scans. J Nucl Med. 2018;59(11):1761–7.
3. Ren S, Jin X, Chan C, Jian Y, Mulnix T, Liu C, et al. Data-driven event-by-event respiratory motion correction using TOF PET list-mode centroid of distribution. Phys Med Biol. 2017;62(12):4741–55.
4. Gillman A, Smith J, Thomas P, Rose S, Dowson N. PET motion correction in context of integrated PET/MR: current techniques, limitations, and future projections. Med Phys. 2017;44(12):e430–e445445.
5. Mukherjee JM, Lindsay C, Mukherjee A, Olivier P, Shao L, King MA, et al. Improved frame-based estimation of head motion in PET brain imaging. Med Phys. 2016;43(5):2443.
6. Schleyer PJ, Dunn JT, Reeves S, Brownings S, Marsden PK, Thielemans K. Detecting and estimating head motion in brain PET acquisitions using raw time-of-flight PET data. Phys Med Biol. 2015;60(16):6441–588.
7. Noonan PJ, Howard J, Hallett WA, Gunn RN. Repurposing the Microsoft Kinect for Windows v2 for external head motion tracking for brain PET. Phys Med Biol. 2015;60(22):8753–66.
8. Jiao J, Searle GE, Schnabel JA, Gunn RN. Impact of image-based motion correction on dopamine D3/D2 receptor occupancy-comparison of groupwise and frame-by-frame registration approaches. EJNMMI Phys. 2015;2(1):15.
9. Huang C, Ackerman JL, Petibon Y, Normandin MD, Brady TJ, El Fakhri G, et al. Motion compensation for brain PET imaging using wireless MR active markers in simultaneous PET-MR: phantom and non-human primate studies. Neuroimage. 2014;91:129–37.
10. Olesen OV, Sullivan JM, Mulnix T, Paulsen RR, Hojgaard L, Roed B, et al. List-mode PET motion correction using markerless head tracking: proof-of-concept with scans of human subject. IEEE Trans Med Imaging. 2013;32(2):200–9.
11. Matsubara K, Ibaraki M, Nakamura K, Yamaguchi H, Umetsu A, Kinoshita F, et al. Impact of subject head motion on quantitative brain (15)O PET and its correction by image-based registration algorithm. Ann Nucl Med. 2013;27(4):335–45.
12. Jin X, Mulnix T, Gallezot JD, Carson RE. Evaluation of motion correction methods in human brain PET imaging–a simulation study based on human motion data. Med Phys. 2013;40(10):102503.
13. Jin X, Chan C, Mulnix T, Panin V, Casey ME, Liu C, et al. List-mode reconstruction for the Biograph mCT with physics modeling and event-by-event motion correction. Phys Med Biol. 2013;58(16):5567–91.
14. Ullisch MG, Scheins JJ, Weirich C, Rota Kops E, Celik A, Tellmann L, et al. MR-based PET motion correction procedure for simultaneous MR-PET neuroimaging of human brain. PLoS One. 2012;7(11):e48149.
15. Olesen OV, Paulsen RR, Hojgaard L, Roed B, Larsen R. Motion tracking for medical imaging: a nonvisible structured light tracking approach. IEEE Trans Med Imaging. 2012;31(1):79–877.
16. Nazarparvar B, Shamsaei M, Rajabi H. Correction of head movements in positron emission tomography using point source tracking system: a simulation study. Ann Nucl Med. 2012;26(1):7–15.
17. Ikari Y, Nishio T, Makishi Y, Miya Y, Ito K, Koeppe RA, et al. Head motion evaluation and correction for PET scans with 18F-FDG in the Japanese Alzheimer's disease neuroimaging initiative (J-ADNI) multi-center study. Ann Nucl Med. 2012;26(7):535–44.
18. Catana C, Benner T, van der Kouwe A, Byars L, Hamm M, Chonde DB, et al. MRI-assisted PET motion correction for neurologic studies in an integrated MR-PET scanner. J Nucl Med. 2011;52(1):154–61.
19. Costes N, Dagher A, Larcher K, Evans AC, Collins DL, Reilhac A. Motion correction of multi-frame PET data in neuroreceptor mapping: simulation based validation. Neuroimage. 2009;47(4):1496–505.
20. Montgomery AJ, Thielemans K, Mehta MA, Turkheimer F, Mustafovic S, Grasby PM. Correction of head movement on PET studies: comparison of methods. J Nucl Med. 2006;47(12):1936–44.
21. Woo SK, Watabe H, Choi Y, Kim KM, Park CC, Bloomfield PM, et al. Sinogram-based motion correction of PET images using optical motion tracking system and list-mode data acquisition. IEEE Trans Nucl Sci. 2004;51(3):782–8.
22. Fulton R, Meikle S, Eberl S, Pfeiffer J, Constable C, Fulham M. Correction for head movements in positron emission tomography using an optical motion-tracking system. IEEE Trans Nucl Sci. 2002;49:116–23.
23. Feng T, Yang D, Zhu W, Dong Y, Li H. Real-time data-driven rigid motion detection and correction for brain scan with listmode PET. In: 2016 IEEE nuclear science symposium, medical imaging conference and room-temperature semiconductor detector workshop (NSS/MIC/RTSD), Strasbourg, 2016. pp. 1–4
24. Karakatsanis NA, Robson PM, Dweck MR, Trivieri MG, Calcagno C, Mani V, et al. PET-driven respiratory phase tracking and self-gating of PET data: clinical demonstration of enhanced lesion detectability in cardiovascular PET/MRI. 2017 ieee nuclear science symposium and medical imaging conference (NSS/MIC); Atlanta, 2017. pp. 1–6

25. Picard Y, Thompson CJ. Motion correction of PET images using multiple acquisition frames. IEEE Trans Med Imaging. 1997;16(2):137–44.
26. Mohy-ud-Din H, Karakatsanis NA, Goddard JS, Baba J, Wills W, Tahari AK, et al. Generalized dynamic PET inter-frame and intra-frame motion correction-Phantom and human validation studies. IEEE Nuclear Science Symposium and Medical Imaging Conference (NSS/MIC); Anaheim, 2012. pp. 3067–78.
27. Raghunath N, Faber TL, Suryanarayanan S, Votaw JR. Motion correction of PET brain images through deconvolution: II. Practical implementation and algorithm optimization. Phys Med Biol. 2009;54(3):813–29.
28. Fulton R, Tellmann L, Pietrzyk U, Winz O, Stangier I, Nickel I, et al. Accuracy of motion correction methods for pet brain imaging. IEEE Trans Med Imaging. 2004;7:4226–300.
29. Jin X, Mulnix T, Sandiego CM, Carson RE. Evaluation of frame-based and event-by-event motion-correction methods for awake monkey brain PET imaging. J Nucl Med. 2014;55(2):287–93.
30. Koshino K, Watabe H, Enmi J, Hirano Y, Zeniya T, Hasegawa S, et al. Effects of patient movement on measurements of myocardial blood flow and viability in resting (1)(5)O-water PET studies. J Nucl Cardiol. 2012;19(3):524–33.
31. Matsumoto K, Kitamura K, Mizuta T, Shimizu K, Murase K, Senda M. Accuracy of attenuation coefficient obtained by 137Cs single-transmission scanning in PET: comparison with conventional germanium line source. Nihon Hosyasen GIjitsu Kakkai Zasshi. 2006;62(2):289–96.
32. Martinez-Moller A, Souvatzoglou M, Delso G, Bundschuh RA, Chefd'hotel C, Ziegler SI, et al. Tissue classification as a potential approach for attenuation correction in whole-body PET/MRI: evaluation with PET/CT data. J Nucl Med. 2009;50(4):520–6.
33. Delso G, Furst S, Jakoby B, Ladebeck R, Ganter C, Nekolla SG, et al. Performance measurements of the Siemens mMR integrated whole-body PET/MR scanner. J Nucl Med. 2011;52(12):1914–22.
34. Shidahara M, Thomas BA, Okamura N, Ibaraki M, Matsubara K, Oyama S, et al. A comparison of five partial volume correction methods for Tau and Amyloid PET imaging with [(18)F] THK5351 and [(11)C]PIB. Ann Nucl Med. 2017;31(7):563–9.
35. Zhang X, Zhou J, Cherry SR, Badawi RD, Qi J. Quantitative image reconstruction for total-body PET imaging using the 2-meter long EXPLORER scanner. Phys Med Biol. 2017;62(6):2465–85.
36. Cherry SR, Badawi RD, Karp JS, Moses WW, Price P, Jones T. Total-body imaging: transforming the role of positron emission tomography. Sci Transl Med. 2017;9(381):eaaf6169.

Affiliations

Takato Inomata[1] · Shoichi Watanuki[2] · Hayato Odagiri[3] · Takeyuki Nambu[4] · Nicolas A. Karakatsanis[5] · Hiroshi Ito[4,6] · Hiroshi Watabe[7] · Manabu Tashiro[2] · Miho Shidahara[2,8]

1 Division of Medical Physics, Tohoku University Graduate School of Medicine, Sendai, Japan

2 Division of Cyclotron Nuclear Medicine, Cyclotron and Radioisotope Center, Tohoku University, Sendai, Japan

3 Department of Diagnostic Radiology, Tohoku University Hospital, Sendai, Japan

4 Advanced Clinical Research Center, Fukushima Medical University, Fukushima, Japan

5 Division of Radiopharmaceutical Sciences, Department of Radiology, Weill Cornell Medical College, Cornell University, Ithaca, USA

6 Department of Radiology and Nuclear Medicine, Fukushima Medical University, Fukushima, Japan

7 Division of Radiation Protection and Safety Control, Cyclotron and Radioisotope Center, Tohoku University, Sendai, Japan

8 Division of Applied Quantum Medical Engineering, Department of Quantum Science and Energy Engineering, Graduate School of Engineering, Tohoku University, Sendai, Japan